New Journal and we have not received input yet 44 (2022) 12–22

Contents lists available at ScienceDirect

Journal of Hydro-environment Research

journal homepage: www.elsevier.com/locate/jher

Research papers

Mean flow, secondary currents and bed shear stress at a 180-degree laboratory bend with and without enhanced permeable groins as an Eco-friendly river structure

Manoochehr Shokrian Hajibehzad [a,*], Mahmood Shafai Bejestan [b], Vito Ferro [c], Rahim Avarand [d]

[a] Researcher at Khuzestan Water and Power Authority (KWPA), Ahvaz, Iran
[b] Hydraulic Structures Department, Shahid Chamran University of Ahvaz, Ahvaz, Iran
[c] Department of Earth and Marine Science, University of Palermo, Via Archirafi 20, 90128 Palermo, Italy
[d] Water Resources Management, Expert at Khuzestan Water and Power Authority (KWPA), Ahvaz, Iran

ARTICLE INFO

Keywords:
Enhanced permeable groin
In-stream structures
River restoration
River bend
Secondary currents
Fish habitat

ABSTRACT

River restoration aims to apply environmentally-friendly structures for bank protection in meandering rivers to restore their natural habitat. Enhanced Permeable Groin (EPG) is a novel river restoration technique that can improve the fish habitat environment in a river system by creating a series of eco-friendly scour pools. This study reports the results of two groups of 3D velocity measurements in a 180-degree channel bend in cases with and without an EPG for clear water conditions to characterize the mechanisms leading to the primary stages of the scouring phenomenon. The analysis revealed that the presence of an EPG amplified the velocity magnitude in the regions near the tip of the vane and increased its value in the middle of the channel 1.13 times the bend without the structure. In addition, the comparison showed that the EPG reduced the velocity magnitude in the recirculation zone by an average of 38%. Secondary currents including main and outer bank cells were observed in the case without the structure. The presence of the EPG in the flow field effectively increased the outer-bank cell strength by 11 times compared to that without the structure. The low-value contours of the bed shear stresses were observed in the zone downstream of the structure for a distance of 6 times the effective length of the structure. Based on the results of this study, the generation of a recirculation zone with low-velocity and shear stress values can provide suitable conditions for aquatic habitats, deep-bodied fish assemblages, aquatic vegetation, shrub roots, and tree roots along the outer bank.

1. Introduction

During the last few decades, groins have been developed and studied as river restoration structures with a significant focus on environmental issues (Rosgen, 2006; D'Agostino and Ferro, 2004; Kurdistani and Pagliara, 2017; Pagliara and Kurdistani, 2017; Ferro et al., 2019; and Shokrian Hajibehzad et al., 2020). These structures have practical applications in stabilizing river alignment, controlling riverbeds, protecting river banks in meander bends, and rebuilding natural habitats (Przedwojski et al., 1995). The presence of a groin-type structure in a flow field alters the mean flow pattern, the strength of secondary currents, and the distribution of bed shear stress which affects the river's morphodynamics, riparian ecology, water quality, and scour-deposition mechanism within the recirculation zone (Bahrami Yarahmadi et al., 2020). Previous studies (Fischer and Paukert, 2008; Pease et al., 2012; Nakagawa, 2014) have shown that the flow velocity in the river affects fish assemblages. Hence, the proper design of these river restoration structures requires an investigation of the flow pattern and an estimate of the velocities or shear stresses experienced by the river environment in their vicinity.

In recent decades, the curvature effects on the flow patterns in river bends have been an interesting topic in river engineering (Julien, 2002). Mockmore (1943) was a pioneer in explaining the flow patterns in curved channels. He measured longitudinal velocity profiles in two 180-degree channel bends and stated that longitudinal velocities in the regions near the inner bank were always greater than those near the outer bank. Rozovskiĭ (1957) performed experimental tests in a 180-degree channel bend to study velocity profiles, flow patterns, and water depth variations. The results indicated that at the entrance of the curved channel, the maximum value of the longitudinal velocity was deflected toward the inner bank and transmitted to the regions along the outer

* Corresponding author.
E-mail address: m.shokrian65@gmail.com (M. Shokrian Hajibehzad).

https://doi.org/10.1016/j.jher.2022.07.004
Received 15 March 2021; Received in revised form 19 September 2021; Accepted 22 July 2022
Available online 25 July 2022

Nomenclature

A_{50}	densimetric particle Froude number;
B	flume width;
C	Chezy coefficient;
d_{50}	mean particle diameter;
d_{84}	size of bed material for which 84 % sampled particles are finer;
d_{16}	size of bed material for which 16 % sampled particles are finer;
H	height of the triangular vane;
h_w	water depth in entrance section;
g	gravity acceleration;
L_e	effective length of the EPG;
L_p	length of permeable groin;
L_t	length of triangular vane;
n	transversal reference axis;
Q	discharge;
s	downstream reference axis;
θ	angle of triangular vane relative to the outer bank tangent;
U	mean velocity of flow at entrance straight section;
$\vec{v}$	mean velocity vector;
v_s	downstream velocity along the channel axis;
v_n	transvers velocity;
v_z	vertical velocity;
V	velocity magnitude;
Y	distance from the inner bank;
z	vertical cross stream direction of flow;
Z	distance from the channel bed;
σ	uniformity factor of the bed material;
τ_b	bed shear stress;
τ_0	mean bed shear stress at the entrance section;
ω_s	streamwise vorticity;
Γ	circulation;
ρ	water density;
ρ_s	density of bed material;

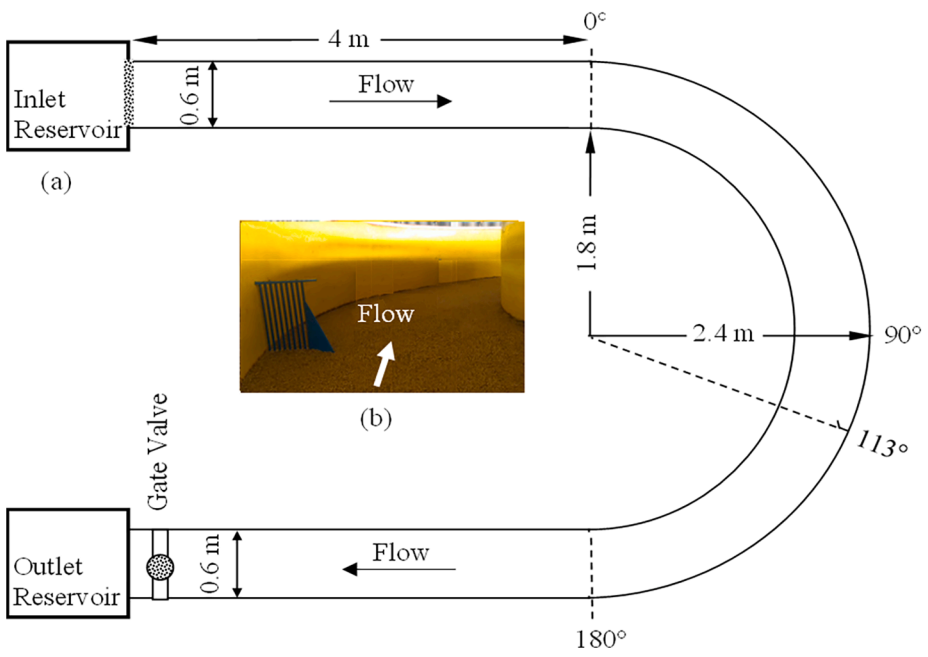

Fig. 1. (a) A schematic plan; and (b) 3D view of the channel bend used in this investigation.

bank while the flow approached the end section of the bend.

The existence of secondary currents in curved channels has been reported in previous studies (Bathurst et al., 1979; Blanckaert and de Vriend, 2004). Different opinions have been developed regarding the function of the outer-bank cell. Bathurst et al. (1979) stated that the outer-bank cell directs high-velocity fluid towards the base of the outer bank and causes its collapse. On the other hand, Blanckaert and Graf (2001) showed that the presence of an outer-bank cell provided a proper condition for the outer bank stability by deflecting the center of the high-velocity zone toward the middle of the channel. Although most of the investigations on the flow pattern around environmentally - friendly structures have been conducted in straight channels (Yeo et al., 2005; Teraguchi et al., 2011; Kang et al., 2011), there have been few experimental investigations on the effects of these structures on the flow field in river bends (Khosronejad et al., 2015; Kang and Sotiropoulos, 2015; Kang et al., 2016). Flow pattern around bank-attached vanes was investigated by Bhuiyan et al. (2010) in a large-scale laboratory model with a developed bed. This investigation showed that triangular vanes generated a counter-rotating circulation cell close to the outer bank, which deflected the high-velocity zone from the outer bank toward the middle of the channel. Bahrami Yarahmadi and Shafai Bejestan (2016) and Bahrami Yarahmadi et al. (2020) also tested the performance of triangular vanes in a 90-degree mild bend and confirmed that these structures generated a counter-rotating circulation cell near the outer bank that counteracted the main circulation cell in the middle of the channel.

Recently, Ferro et al. (2019) introduced a novel environmentally-friendly river restoration technique called enhanced permeable groin. Because the effect of this newly-introduced structure on the flow field has not yet been studied, the main aim of the present study was to

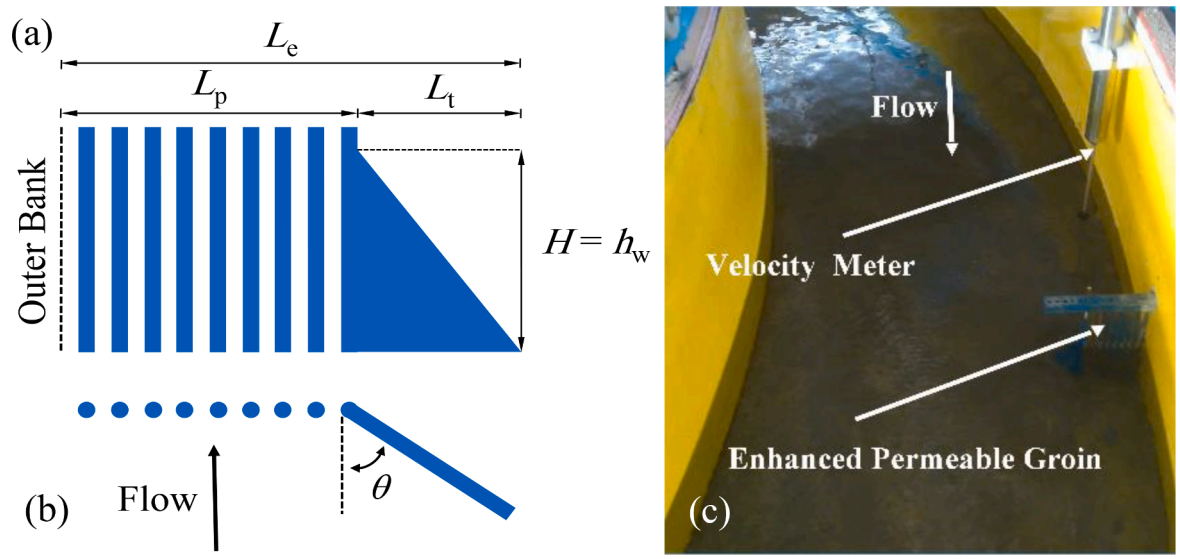

Fig. 2. (a) Side and (b) plan views of an EPG; (c) a view of the velocity meter.

Table 1
Experimental conditions for the cases with and without the EPG.

Experiment	discharge Q (m^3/s)	water depth $h_w = H$(m)	d_{50} (mm)	A_{50}	L_p (m)	L_t (m)	θ (degree)	Groin permeability (%)	number of grid points
Without EPG	0.01875	0.12	0.088	2.18	–	–	–	–	360
With EPG	0.01875	0.12	0.088	2.18	0.09	0.05	50	50	870

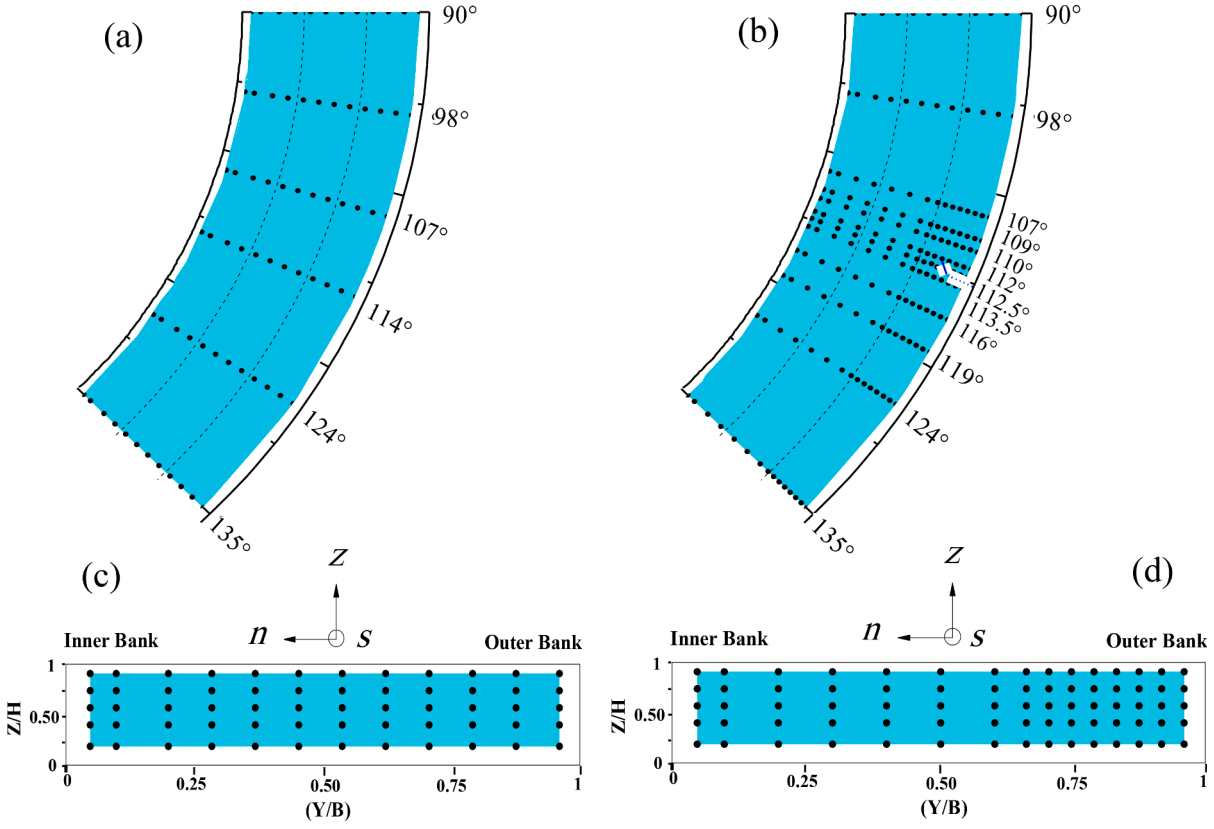

Fig. 3. Plan and sectional illustrations of the measurement grids in cases with (b and d) and without (a and c) an EPG.

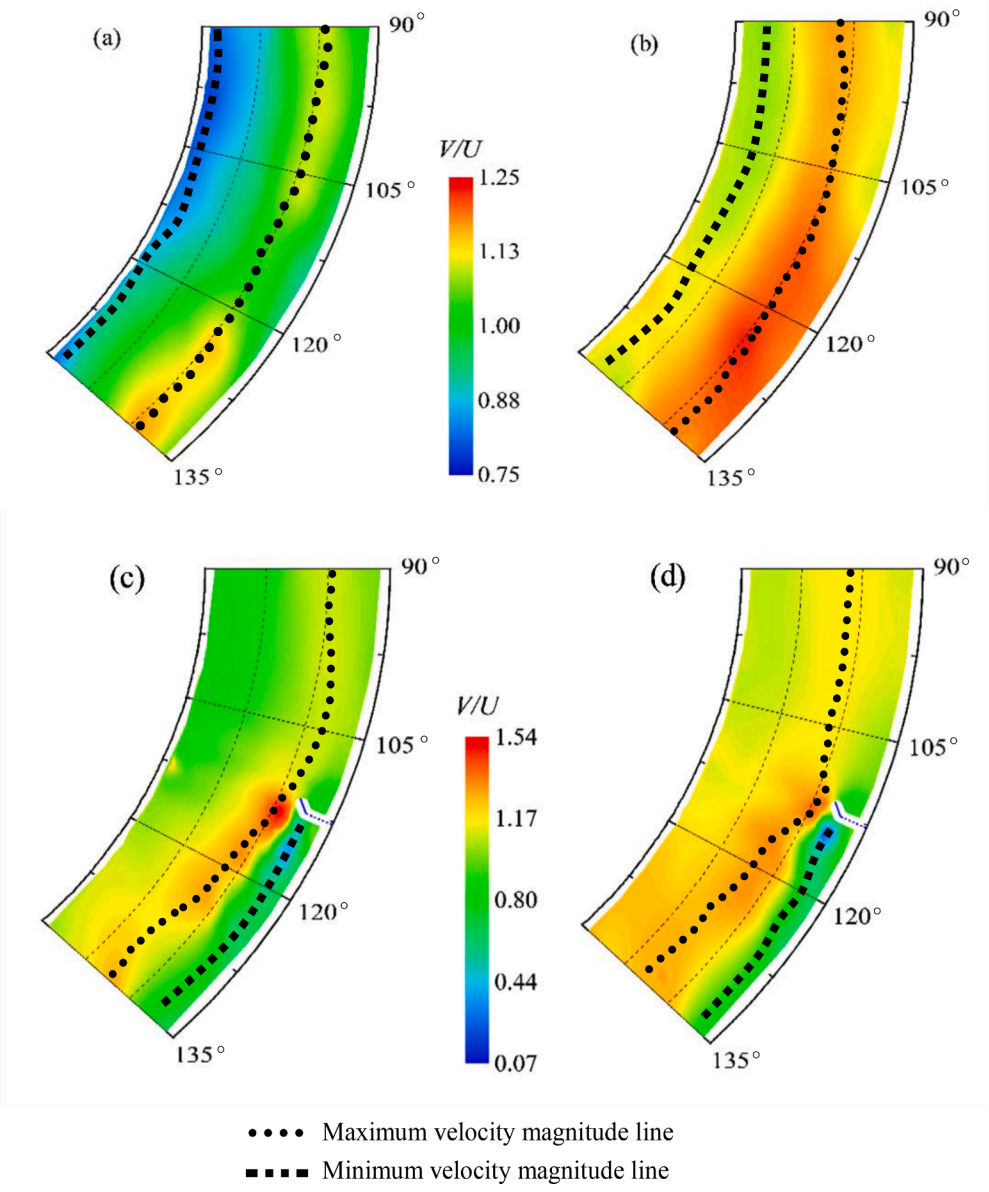

Fig. 4. Contours of the normalized velocity magnitude V at $Z/H = 0.208$ (b and d) and $Z/H = 0.916$ (a and c) in the bend with (c and d) and without (a and b) the enhanced permeable groin.

investigate the mean flow pattern, strength of secondary currents, and bed shear stress around this structure to understand the mechanisms leading to scour in the early stages of the scouring process.

2. Experimental setup

Experimental runs were conducted in a 180-degree steel wall mild channel bend, having a width B equal to 0.6 m, a mean radius of 2.1 m, a bed material with $d_{50} = 0.00088$ m, and a uniformity factor of $\sigma = (d_{84}/d_{16})^{0.5} = 1.7$. The thickness of the bed material was equal to 0.25 m. A schematic plan with all the details of the channel bend is shown in Fig. 1. A downstream gate valve was used to control the flow depth in the channel, and an electromagnetic flowmeter with an accuracy of ±0.1 % was installed in the inlet pipe to measure the flow rate. The bed material was surfaced using a bed leveler. According to Koken and Constantinescu (2008), a considerable quantity of scour around groin-type structures occurs within a short time after installation, and it is necessary to identify the flow pattern in this stage. Moreover, the general features of the flow pattern around groins are very similar in the early and late stages of the scouring process (Kashyap, 2012). Hence, the channel bed was fixed by spraying cement and albumen to investigate the mechanisms leading to scouring in a flat fixed sediment bed with no sediment movement. In Fig. 2a, L_e is the effective length of the EPG, L_p is the length of the permeable groin, L_t is the effective length of the vane, H is the height of the triangular vane (equal to h_w) and θ represents the vane angle with the tangent line of the outer bank. The geometry of the enhanced permeable groin (Fig. 2a) was selected according to the study by Ferro et al (2019). Their results showed that the enhanced permeable groin with the geometry of $L_t/L_p = 0.55$ ($L_t = 0.05$ m and $L_p = 0.09$ m) and $\theta = 50^\circ$ has the best performance from the sedimentological and economical point of views. The total effective length L_e of the structure was 0.14 m which was installed at the 113-degree section of the bend (Fig. 1a).

Two groups of experiments were carried out with and without an EPG to sample the 3D-velocity components in the bend (Table 1). For both groups, the water depth h_w at the entry straight section of the bend was constant (0.12 m) and the particle Froude number A_{50} defined by

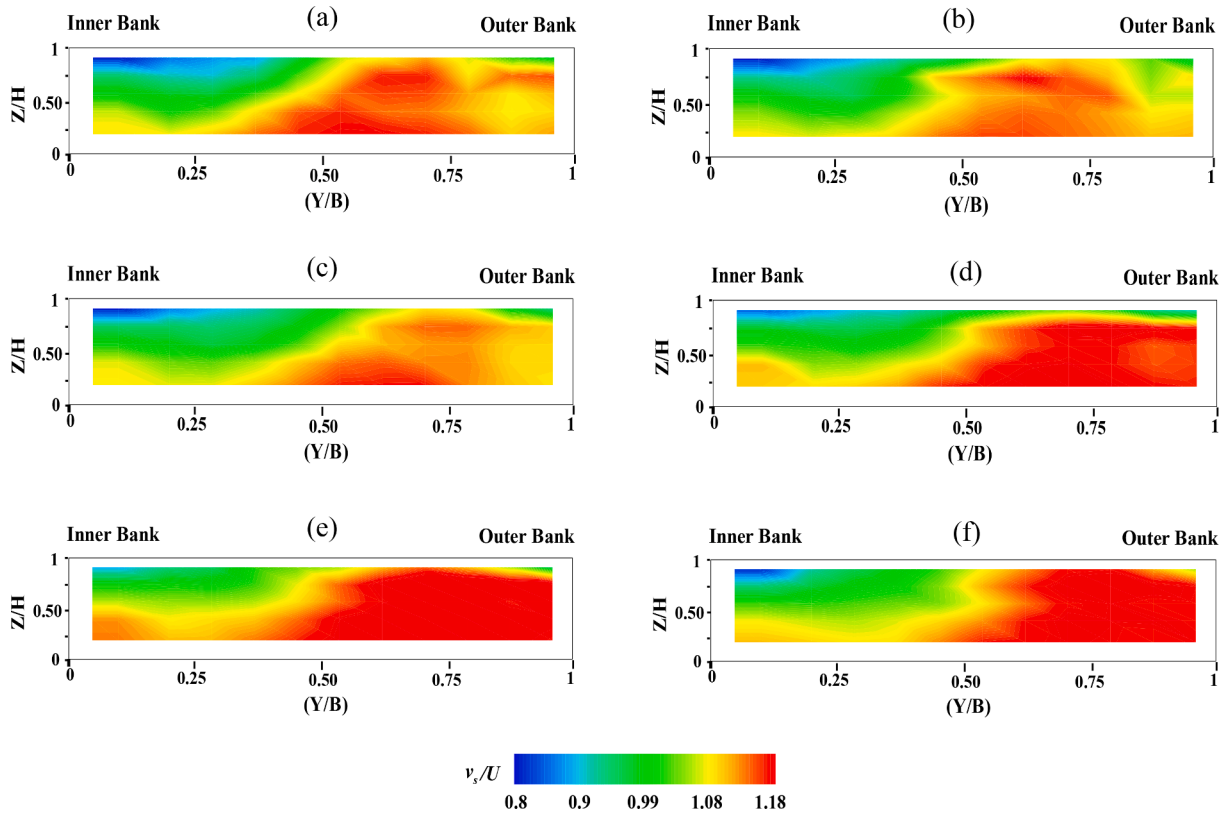

Fig. 5. Contour plots of normalized longitudinal velocity (v_s/U) at different sections in the bend without the EPG: (a) 90°; (b) 98°; (c) 107°; (d) 114°; (e) 124°; (f) 135°.

Eq. (1) (D'Agostino and Ferro, 2004) was considered equal to 2.18.

$$A_{50} = \frac{Q}{Bh_w\left[gd_{50}\left(\frac{\rho_s-\rho}{\rho}\right)\right]^{1/2}} \quad (1)$$

Here, B is the channel width, Q is the discharge, h_w is the water depth, ρ is the water density, g is the gravitational acceleration, ρ_s is the bed material density, and d_{50} is the median particle diameter.

The 3D velocity components were sampled using an electromagnetic current velocity meter (model: ACM3-RS/ACM-4IF) with an accuracy of ±2 % (Fig. 2b). A sampling frequency of 60 Hz with an acquisition time of 180 s was considered. Two types of non-uniform and uniform 3D grids were designed to measure the velocity components $\vec{v} = (v_s, v_n, v_z)$ in the cylindrical coordinate system s, n and z for the experiments with and without the structure, respectively (Fig. 3). In this system, s, n and z represent the downstream direction along the channel axis, transverse axis from the outer sidewall, and vertical axis from the bed surface, respectively. For both groups of experiments, vertical velocity profiles were sampled at five normalized water depths Z/H (0.208, 0.416, 0.583, 0.75 and 0.916) from the channel bed. In the case without the structure, the normalized lateral distances from the inner bank Y/B (0.05, 0.1, 0.2, 0.283, 0.366, 0.45, 0.6, 0.7, 0.783, 0.866 and 0.95) were selected (Fig. 3a and c). More normalized lateral distances (0.05, 0.1, 0.2, 0.3, 0.4, 0.5, 0.6, 0.658, 0.7, 0.741, 0.783, 0.825, 0.866, 0.908 and 0.95) were also considered for the case with the EPG (Fig. 3b and d). In the bend without the EPG, six different normalized longitudinal distances (0, 2.38, 5.07, 7.76, 10.15, 13.43L_e) from the bend apex (shown in Fig. 3a in degrees) were selected to measure the velocity components. For the EPG, seven (0.15, 0.3, 0.6, 0.9, 5.07, and 6.86L_e) and five (0.15, 0.375, 1.8, 3.28 and 6.57L_e) normalized longitudinal distances from the groin section (113-degree) were considered for the velocity sampling in the areas upstream and downstream of the structure, respectively.

Bahrami Yarahmadi et al. (2020) and Bhuiyan et al. (2010) reported that the most comprehensive amplification of the velocity components occurs in the areas near the tip of the vane. Therefore, in the bend with the EPG, a non-uniform measurement grid was used to sample the velocity components to improve the accuracy and to conduct a more detailed study of the flow pattern. In other words, when approaching the structure, the distance between the measuring points decreases in the longitudinal and transverse directions.

The minimum space between the probe of the velocity meter and the solid boundaries of the flow field was 0.025 m because of the limitations of the velocity meter. A traversing operation was designed to locate the velocity meter with an accuracy of 0.001 m in the transverse, vertical, and streamwise directions.

3. Results and discussion

3.1. Mean flow pattern

Fig. 4 shows the contours of the normalized velocity magnitude $V = \sqrt{v_s^2 + v_n^2 + v_z^2}$ at the horizontal planes at $Z/H = 0.208$ (near bed), and $Z/H = 0.916$ (near the surface) in the bend with (c and d) and without (a and b) the EPG. In this Figure, U represents the mean velocity of the flow at the entry straight segment of the bend which is equal to the ratio between the flow rate Q and the section area ($U = Q/Bh_w$).

Fig. 4(a and c) display the results near the surface velocity magnitude and the Figures on the right (b and d) display the results near the bed. As shown, the normalized velocity magnitude V/U for the bend without the structure (a and b) decreases from the outer to the inner bank at both horizontal planes, and high velocities occur in the area near the outer bank, especially at the near-bed level. Furthermore, the comparison between the velocity magnitude of both horizontal planes reveals that the center of maximum velocity magnitude forms in the regions near the

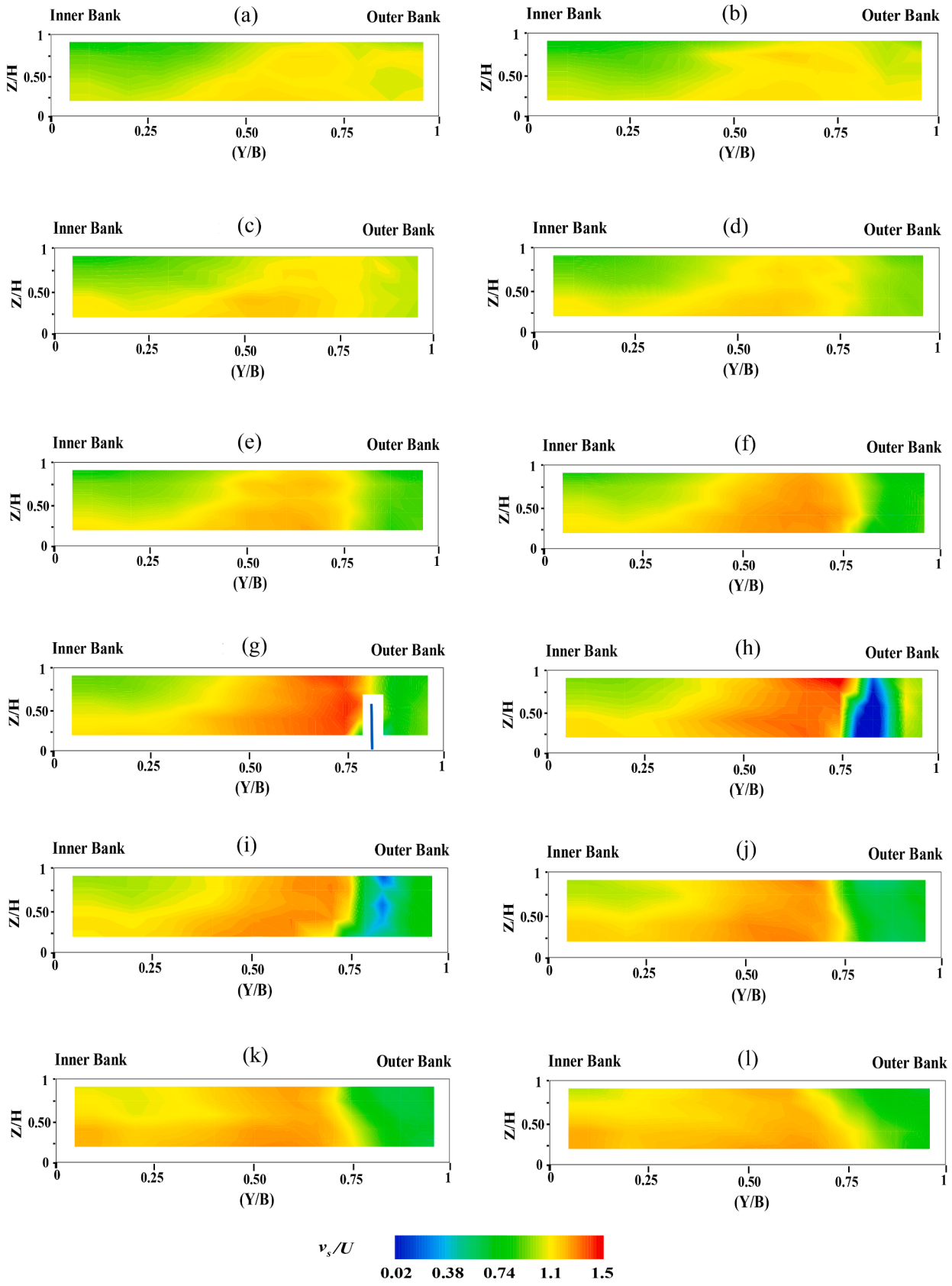

Fig. 6. Contour plots of normalized longitudinal velocity (v_s/U) at different sections in the bend with an EPG: (a) 90°; (b) 98°; (c) 107°; (d) 109°; (e) 110°; (f) 112°; (g) 112.5°; (h) 113.5°; (i) 116°; (j) 119°; (k) 124°; (l) 135°.

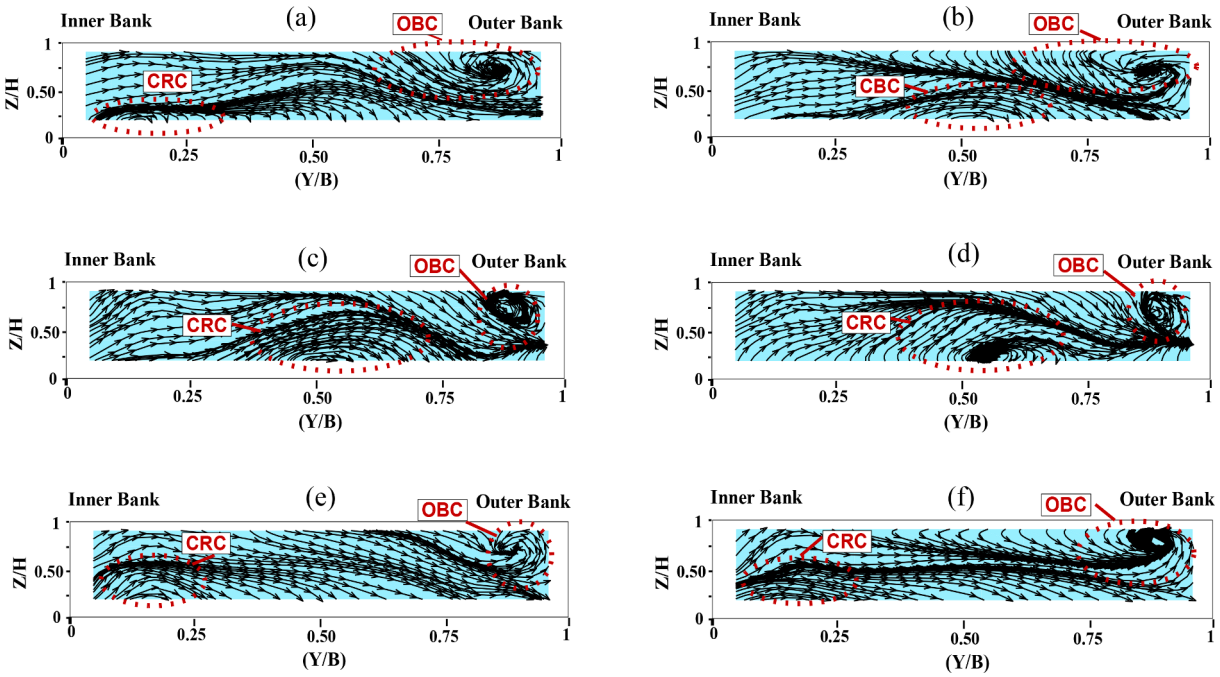

Fig. 7. 2-D streamlines at different sections in the bend without the EPG: (a) 90°; (b) 98°; (c) 107°; (d) 114°; (e) 124°; (f) 135°.

bed, and its value is on average 1.17 times the regions near the free surface. This result is in agreement with that of Blanckaert and Graf (2001). The line of the minimum velocity magnitude is closer to the inner bank in the near surface regions. Fig. 4(c and d) also show that the presence of the EPG considerably alters the distribution of the velocity magnitude within the bend, particularly in the recirculation zone behind the structure. The deviation and constriction of the main flow due to the presence of the EPG cause a strong amplification of velocity magnitude in the regions near the tip of the triangular vane and increase the average velocity magnitude in the middle of the channel 1.13 times the bend without the structure. The line of the maximum velocity magnitude relocates from the outer bank toward the middle of the channel in both horizontal planes. The comparison between the cases with and without the structure reveals that the EPG reduces the velocity magnitude in the recirculation zone along the outer bank by 38 %. Owing to this velocity reduction, the line of the minimum velocity magnitude relocates from the inner bank toward the outer bank downstream of the structure, compared to the bend without the EPG. Similar to the bend without the EPG, the center of the high velocity magnitude in the regions near the bed was also found to be 1.09 times the velocity near the surface. Outside the shear layer, a region of diverted flow is formed where the acceleration of the flow increases as it passes the structure. As shown, the effect of the structure on the flow field was considerable. The large amplification of the velocity magnitude occurs in the bend with the EPG between sections 114- and 120-degree. From an environmental point of view, the generation of a low-velocity recirculation zone near the outer bank can provide proper conditions for aquatic habitats (Kang et al., 2012). There is a strong positive relationship between low-velocity microhabitats and fish assemblages, aquatic vegetation, shrub roots, and tree roots along the bank (Bower and Winemiller, 2019; Enders et al., 2005). Low-velocity habitats include more fish assemblages for most traits, especially fishes with greater body depth such as centrar-chids and cichlids (Bower and Winemiller, 2019). The results of Fig. 4 show that the EPG generates a proper low-velocity habitat along the outer bank with a maximum length of $6L_e$ and a maximum width of $0.2B$. Moreover, an environmentally-friendly river restoration structure must provide suitable living space for all aquatic species. Fishes with average anal fin height, head length, pectoral fin length, pectoral fin width, and pelvic fin length tend to occupy high-velocity habitats (Bower and Winemiller, 2019). The presence of the EPG also generates high-velocity habitats in the regions near the tip of the vane and in the middle of the channel.

The contour plots of the normalized longitudinal velocity (v_s/U) for the sections 90–135-degree of the bend without and with an EPG are depicted in Figs. 5 and 6, respectively. In these Figs, the vertical axis displays the normalized water depth (Z/H) and the horizontal axis indicates the normalized lateral distance from the inner bank (Y/B). Fig. 5 shows that the maximum and minimum longitudinal velocities occur in zones close to the outer and inner sidewalls, respectively. As a result of the centrifugal force, the center of the high longitudinal velocity zone gradually moves toward the outer bank and finally reaches the bank at the 114-degree section (Fig. 5d).

Fig. 6 shows that in sections 107–112.5-degree upstream of the structure (Fig. 6c–g), the longitudinal velocity decreases along the outer bank. Because of this velocity reduction and the deviation of flow by the structure, the longitudinal velocity increases in the middle of the channel, especially in the regions near the surface. Compared to the bend without the structure, the amplification of longitudinal velocity increases in the downstream direction and a maximum value of 40 % occurs in the cross section of the structure. As the flow passes the enhanced permeable groin, and in the 113.5-degree section (Fig. 6h), a triangular zone of low longitudinal velocity is observed behind the triangular vane. As shown, this triangular zone gradually disappears by moving away from the structure and a uniform zone of low longitudinal velocity is formed along the outer bank. The generation of such a low velocity zone near the outer bank limits the channel width and extends the center of the high longitudinal velocity zone toward the regions near the inner bank. This function of the enhanced permeable groin effectively protects the outer bank and can be of great help in improving the sedimentation near the outer bank. The rate of sedimentation along the outer bank is also a significant factor in the river environment. Extreme sedimentation downstream of impermeable groins, creating large horizontal vortices and still water conditions, negatively affects aquatic habitats (Bhuiyan et al., 2010). Compared to the impermeable groin, the sedimentation rate is lower for the EPG owing to the permeability. The generation of various shear layers downstream of the permeable groin piles and the triangular vane can improve the aeration conditions, which benefits the microhabitat. Suitable sedimentation, uniform velocity

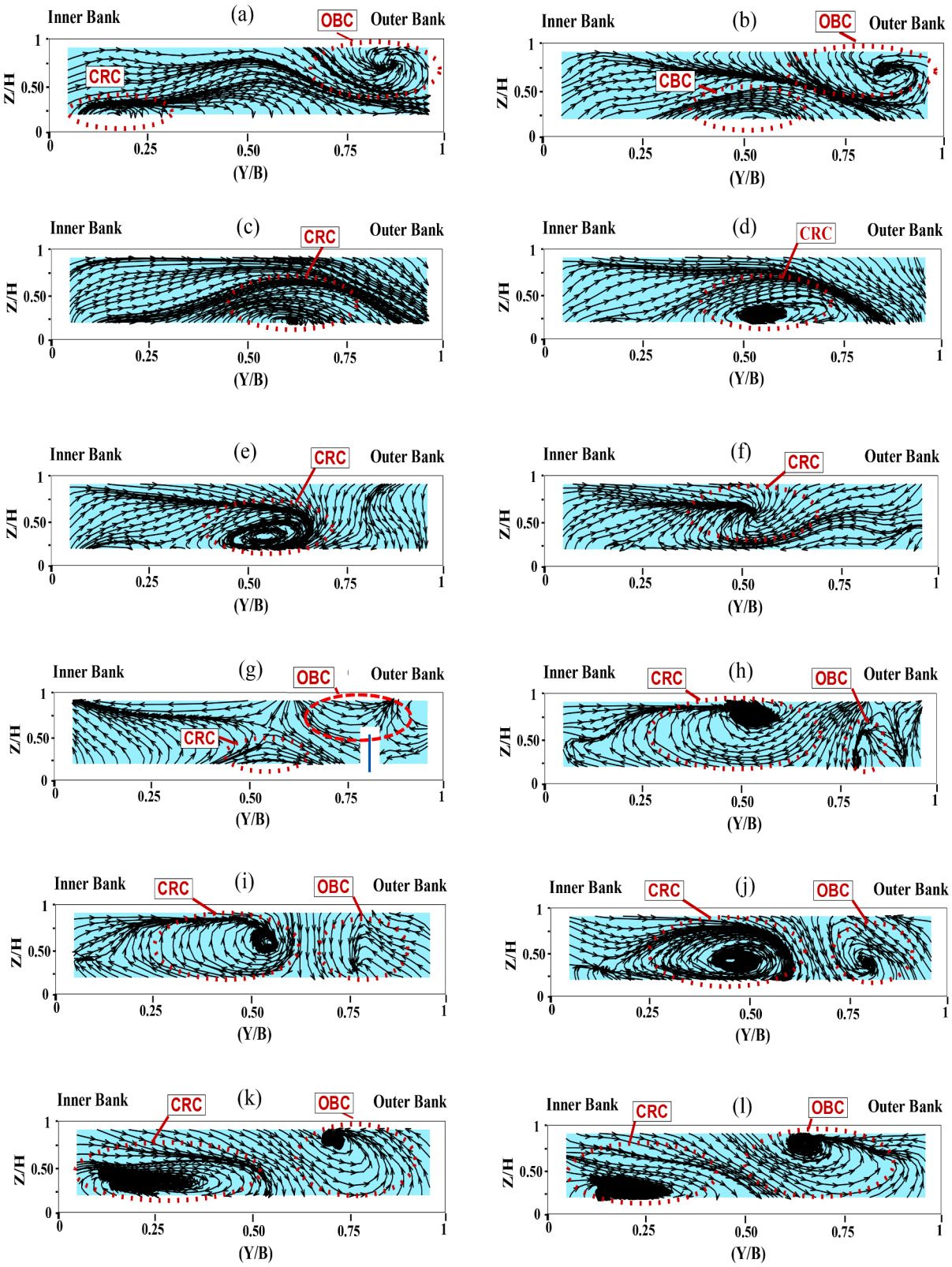

Fig. 8. 2-D streamlines at different sections in the bend with the EPG: (a) 90°; (b) 98°; (c) 107°; (d) 109°; (e) 110°; (f) 112°; (g) 112.5°; (h) 113.5°; (i) 116°; (j) 119°; (k) 124°; (l) 135°.

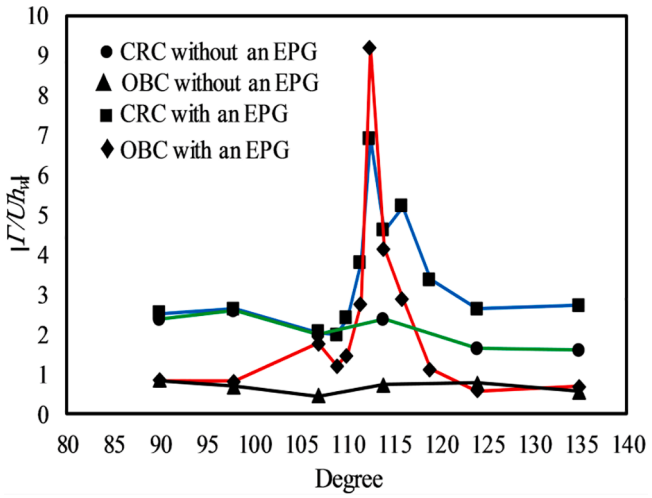

Fig. 9. Variation of normalized circulation strength for both CRC and OBC in the bend with and without an EPG.

reduction in the depth and along the outer bank create a proper living space for underwater organisms. According to Kang et al. (2012), a velocity reduction in the range of $0 < v_s/U < 0.5$ provides a suitable living environment for most fish traits. The results in Fig. 6 indicate that the rate of velocity reduction downstream of the EPG is between 0.02 and 0.5.

3.2. Secondary currents

The principal feature of the flow in river bends is the development of secondary currents. Both the center-region cell (CRC) and the outer-bank cell (OBC) were observed in the experiments. As shown in Fig. 7, both circulation cells were formed in the bend without the EPG. The center-region cells are more visible in the 107- and 114-degree sections (Fig. 7c and d). The core of the OBC is situated in the regions near the surface, and beside the outer bank, suggesting that such a cell has a significant role in reducing or increasing the scour at the outer bank. The results show that the OBC in the bend without the structure preserves the outer bank partly in the regions near the surface, while it directs high-velocity fluid particles toward the outer bank toe near the bed regions. According to Bathurst et al (1979), this problem can endanger the bank's stability.

The streamline patterns around the EPG are shown in Fig. 8. The analysis showed that the enhanced permeable groin had no significant effects on the flow field upstream of the 107-degree section (Fig. 8c). Fig. 8 demonstrates that the EPG affects the size and location of both CRC and OBC and prevents high-velocity fluid particles from reaching the base of the outer bank. As a result, the EPG can protect the upstream zone of the outer bank for a length equal to 1.5 L_e, while there is no OBC between the 107- and 112-degree sections. After the 109-degree section (Fig. 8d), the characteristics of the CRC changed. By approaching the structure on the upstream side, the CRC slightly disappears and complex flow patterns are formed in the bend, as shown in the 112.5-degree section (Fig. 8g). In the first section downstream of the structure (Fig. 8h), a fully complex flow pattern is formed and a small OBC develops behind the vane. Furthermore, a CRC can be found in the middle of the channel away from the structure. The location of the CRC relocates toward the water surface, compared to upstream of the structure. Moreover, the position of the OBC gradually moves toward the channel bottom and affects the size and location of the CRC. As shown in the 135-degree section (Fig. 8l), the CRC is relocated toward the inner bank because of a strong OBC. This suggests that the presence of the EPG induces the generation of the OBC and effectively protects the outer bank near the bed and surface regions. Furthermore, an upward flow forms behind the permeable part of the structure, which can facilitate the deposition of suspended sediments. Compared to the bend without the EPG, the size and location of the OBC is effective enough to deflect high-velocity fluid particles away from the outer bank. As shown in the 116-, 119-, 124- and 135-degree sections (Fig. 8i to l), high-velocity zones were observed in the middle of the channel between the two circulation cells, which increased the shear stress, turbulence and scour in the middle of the channel. The higher levels of turbulent kinetic energy in the shear layer between the center region and the outer bank cells play a very important role in the transport of eroded sediments toward the outer bank. This high level of turbulent kinetic energy is due to the formation of turbulent vortices that extend over the entire depth of the flow (Bhuiyan et al., 2010). This function of enhanced permeable groin can improve fish habitat. According to previous investigations (Liao et al, 2003; Enders et al, 2005), turbulence plays an important role in the feeding behavior and swimming costs of fish. Highly turbulent environments can reduce the swimming costs during attacks by approximately 42 %, compared to low turbulence conditions.

The variation in circulation strength for both the CRC and the OBC along the bend in the cases with and without the EPG are shown in Fig. 9. According to Daily and Harleman (1966), the two dimensional streamwise vorticity (ω_s) in a cell as large as $\Delta n \times \Delta z$ in a cross- section perpendicular to the channel axis (s) can be calculated as follows:

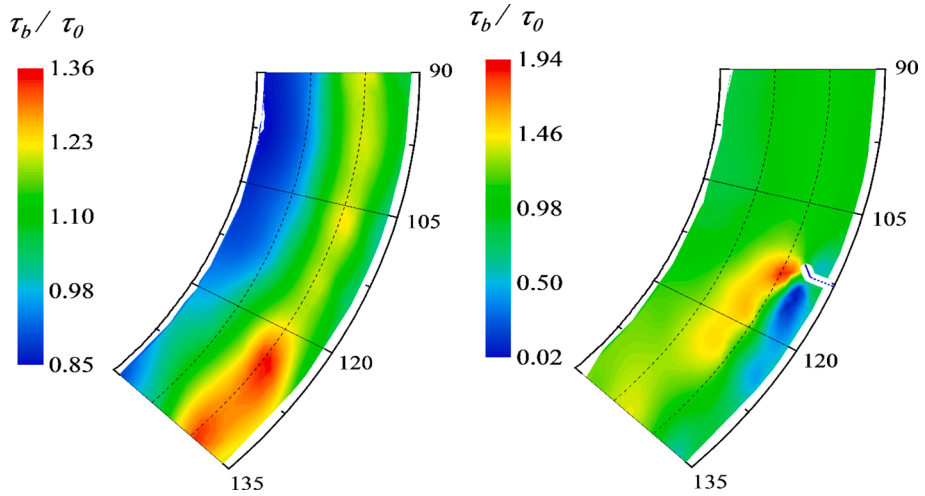

Fig.10. Distribution of bed shear stress in the bend; (a) without and; (b) with the EPG.

$$\omega_s = \frac{1}{2}\left(\frac{\partial v_n}{\partial z} - \frac{\partial v_z}{\partial n}\right) \quad (2)$$

Here, v_n and v_z are the transverse and vertical velocities, respectively. The cross-stream circulation magnitude Γ represents the sum of the streamwise vorticity over the sectional area. In other words, Γ + and Γ − are the total positive ($\omega_s > 0$) and negative ($\omega_s < 0$) circulations calculated by Eq.2, respectively. Facing the upstream direction, positive and negative ω_s rotate in the clockwise (CRC) and counterclockwise (OBC) directions, respectively.

The variation in the normalized circulation strength $|\Gamma/Uh_w|$ in the bend with and without EPG is shown in Fig. 9. It can be seen that, in the case without the EPG, there is no rapid change in the clockwise and counterclockwise circulations between the 90- and 135-degree sections. In all sections, the magnitude of clockwise circulation was observed to be more than counterclockwise. Fig. 9 suggests that by moving from the bend apex downstream, the difference between the magnitudes of clockwise and counterclockwise circulations gradually decreases. According to Zeng et al. (2008), the magnitude of circulation Γ is a very important parameter because it controls the nonlinear interactions between the longitudinal and transverse velocities. In other words, the transverse transport of longitudinal momentum is a strong function of the circulation magnitude. Therefore, the gradual decrease in clockwise circulation decreases the outward transport of longitudinal momentum between the 90- and 135-degree sections.

The distribution of clockwise and counterclockwise circulations for the bend with an EPG is also shown in Fig. 9. Both clockwise and counterclockwise circulations peaked at approximately the 112.5-degree section close to the tip of the triangular vane. The levels of the clockwise and counterclockwise circulation magnitudes are 3 and 11 times greater than those for the case without the structure, respectively. These high levels of circulation magnitude near the tip of the triangular vane are mainly responsible for the occurrence of the maximum scour depth in this region due to a strong shear layer formed between the two circulation cells, as has been reported by Ferro et al. (2019). The results show a rapid decrease in circulation compared to the 112.5-degree section, but there is still a considerable circulation strength in the downstream regions. For the regions upstream of the 110-degree section, the magnitude of clockwise circulation seems to be equal to the case without the structure, while its value increases in the downstream regions.

3.3. Bed shear stress

Fig. 10 shows the variation of the normalized bed shear stress (τ_b/τ_0) in the bend with (b) and without (a) the EPG. Bed shear stresses in the longitudinal and transverse directions were calculated using the following equations proposed by Molls and Chaudhry, (1995):

$$\tau_{bs} = \frac{\rho g}{C^2}\bar{v}_s\sqrt{\bar{v}_s^2 + \bar{v}_n^2} \quad (3)$$

$$\tau_{bn} = \frac{\rho g}{C^2}\bar{v}_n\sqrt{\bar{v}_s^2 + \bar{v}_n^2} \quad (4)$$

in which Eqs. (3) and (4) represent the bed shear stresses (N/m^2) in the longitudinal s and transverse n directions, respectively. In these equations, C is the Chezy coefficient, $\bar{v}_s$ is depth-averaged longitudinal velocity (m/s),$\bar{v}_n$ is depth-averaged transverse velocity (m/s), g is gravity acceleration (9.81 m/s^2), and ρ is water density. The total bed shear stress is computed as follows:

$$\tau_b = \sqrt{\tau_{bs}^2 + \tau_{bn}^2} \quad (5)$$

The total bed shear stress calculated by Eq.5 was normalized by the mean bed shear stress at the straight entrance section of the bend (τ_0). Fig. 10a shows that the maximum bed shear stress occurred in the regions near the outer bank between the 120- and 135-degree sections. Furthermore, it can be seen that the regions with the lowest bed shear stress are concentrated near the inner bank, where the eroded sediments are mainly deposited. From the approximately 120-degree section, the shear stress gradually increases and finally reaches its maximum value downstream of the 125-degree section.

The distribution of the bed shear stress in the bend with EPG is shown in Fig. 10b. The results indicate that the maximum values of the bed shear stresses occur in the regions near the tip of the triangular vane and in the middle of the channel between the 114- and 125-degree sections. Compared to the bend without the structure, the EPG amplifies the bed shear stress by an average of 1.6 times in the channel center. Moreover, it was found that the presence of the EPG in the flow field reduced the maximum shear stress in the regions behind the structure by approximately 46 %. Areas with low shear stress are suitable environments for fish with greater body depth because the bioenergetic costs are lower because of the low drag force (Bower and Winemiller, 2019). Furthermore, the spaces between the permeable groin piles allow fish to migrate upstream during the spawning season.

The results in Fig. 10 reveal that the maximum bed shear stresses were formed in the zone between the CRC and OBC. In the case of the EPG, the OBC line relocates from the outer bank toward the channel middle, shifting the line of maximum shear stress toward the middle of the channel. The results of erosion and sedimentation processes in the presence of the EPG reported by Ferro et al. (2019) confirmed the distribution of bed shear stress in this study. They reported that the maximum scour depth occurs close to the tip of the triangular vane, where the high levels of bed shear stress are concentrated, while the sediment deposition forms in the zones downstream of the structure with low levels of shear stress. A series of eco-friendly scour holes formed near the tip of the vanes can be used as swimming pools for different species of fish, as reported by Ferro et al (2019) and Shokrian Hajibehzad et al. (2020).

4. Conclusions

The proper design of river restoration structures is a very important issue from an eco-friendly point of view. The presence of a river restoration structure alters the flow field near the structure and affects the scour-deposition mechanisms in the recirculation zone. In the present study, experimental tests were conducted to investigate the flow patterns, circulation strength, and bed shear stress distribution around a novel river restoration technique called enhanced permeable groin to analyze the mechanisms leading to scouring in the initial stages. In the bend without the structure, the central region and outer bank cells were observed. The results showed that the outer bank cell forms in the region near the water surface and can only partially protect the outer bank in these regions. The investigations showed that the outer bank cell in this case directs high-velocity fluid particles toward the toe of the outer bank and increases the risk of its collapse. With the structure in the bend, the investigations confirmed that the new structure can effectively deflect the core of the high-velocity zone toward the middle of the channel to protect the outer bank. The longitudinal velocity within the recirculation zone downstream of the structure was reduced to approximately 38 %. The analysis showed that, in comparison with the bend without the structure, the enhanced permeable groin increases the strength of the outer bank cell by as much as approximately 11 times. Moreover, high levels of bed shear stress were observed in the zone near the tip of the triangular vane. In the case of the structure, the results confirmed that low levels of bed shear stress were formed downstream of the structure where eroded sediments were deposited. The implementation of the EPG in the outer bank of a river bend can improve deep-bodied fish assemblages, aquatic vegetation, shrub roots, and tree roots along the bank. Furthermore, the generation of various shear layers downstream of the permeable part of the structure enhances the aeration conditions, which benefits the aquatic habitat. The results of this study can be useful for the proper design of the enhanced permeable groin as a newly-introduced

river restoration structure and lead to more attention directed toward this eco-friendly and cost-effective technique.

Declaration of Competing Interest

The authors declare that they have no known competing financial interests or personal relationships that could have appeared to influence the work reported in this paper.

Acknowledgement

The authors would like to thank the Iran National Science Foundation (INSF) for financial support under Grant No. 96005198.

References

Bahrami Yarahmadi, M., Shafai Bejestan, M., 2016. Sediment management and flow patterns at river bend due to triangular vanes attached to the bank. J. Hydrol.-Environ. Res. 10, 64–75.
Bahrami Yarahmadi, M., Shafai Bejestan, M., Pagliara, S., 2020. An experimental study on the secondary flows and bed shear stress at a 90-degree mild bend with and without triangular vanes. J. Hydrol.-Environ. Res. 33, 1–9.
Bathurst, J.C., Hey, R.D., Thorne, C.R., 1979. Secondary flow and shear stress at river bends. J. Hydraulic Divis. 105 (10), 1277–1295.
Bhuiyan, F., Hey, R.D., Wormleaton, P.R., 2010. Bank-attached vanes for bank erosion control and restoration of river meanders. J. Hydraul. Eng. 136 (9), 583–596.
Blanckaert, K., de Vriend, H., 2004. Secondary flow in sharp open-channel bends. J. Fluid Mech. 498 (12), 353–380.
Blanckaert, K., Graf, W.H., 2001. Mean flow and turbulence in open-channel bend. J. Hydraul. Eng. 127 (10), 835–847.
Bower, L.M., Winemiller, K.O., 2019. Fish assemblage convergence along stream environmental gradients: an intercontinental analysis. Ecography 42 (10), 1691–1702.
D'Agostino, V., Ferro, V., 2004. Scour on alluvial bed downstream of grade-control structures. J. Hydraul. Eng. 130 (1), 24–37.
Daily, W., Harleman, D., 1966. *Fluid dynamics*. Addison-Wesley. Publishing Company.
Enders, E.C., Buffin-Bélanger, T., Boisclair, D., Roy, A.G., 2005. The feeding behaviour of juvenile Atlantic salmon in relation to turbulent flow. J. Fish Biol. 66 (1), 242–253.
Ferro, V., Shokrian-Hajibehzad, M., Shafai-Bejestan, M., Kashefipour, S.M., 2019. Scour around a permeable groin combined with a triangular vane in river bends. J. Irrig. Drain. Eng. 145 (3), 04019003.
Fischer, J.R., Paukert, C.P., 2008. Habitat relationships with fish assemblages in minimally disturbed Great Plains regions. Eco. Fresh. Fish. 17 (4), 597–609.
Julien, P.Y., 2002. River Mechanics. Cambridge University Press.
Kang, S., Sotiropoulos, F., 2015. Numerical study of flow dynamics around a stream restoration structure in a meandering channel. J. Hydraul. Res. 53 (2), 178–185.
Kang, S., Hill, C., Sotiropoulos, F., 2016. On the turbulent flow structure around an instream structure with realistic geometry. Water Resources Res. 52 (10), 7869–7891.
Kang, J., Yeo, H., Kim, S., Ji, U., 2011. Permeability effects of single groin on flow characteristics. J. Hydraul. Res. 49 (6), 728–735.
Kang, J., Yeo, H., Jung, S., 2012. Flow characteristic variations on groyne types for aquatic habitats. Sci. Res. 4 (11), 809–815.
Kashyap, S., 2012. A 3-D Numerical Study of Flow, Coherent Structures, and Mechanisms Leading to Scour in a High Curvature 135 Channel Bend With and Without Submerged Groynes. University of Ottawa (Canada).
Khosronejad, A., Kozarek, J.L., Diplas, P., Sotiropoulos, F., 2015. Simulation-based optimization of in-stream structures design: J-hook vanes. J. Hydraul. Res. 53 (5), 588–608.
Koken, M., Constantinescu, G., 2008. An investigation of the flow and scour mechanisms around isolated spur dikes in a shallow open channel: 1. Conditions corresponding to the initiation of the erosion and deposition process. Water Resour. Res. 44 (8), 1–19.
Kurdistani, S.M., Pagliara, S., 2017. Experimental study on cross vane scour morphology in curved horizontal channels. J. Irrig. Drain. Eng. 143 (7), 04017013(9).
Liao, J.C., Beal, D.N., Lauder, G.V., Triantafyllou, M.S., 2003. Fish exploiting vortices decrease muscle activity. Science 302 (5650), 1566–1569.
Mockmore, C., 1943. Flow around bends in stable channels. Trans. Am. Soc. Civ. Eng 109 (12), 593–628.
Molls, T., Chaudhry, M.H., 1995. Depth-averaged open-channel flow model. J. Hydraul. Eng. 121 (6), 453–465.
Nakagawa, H., 2014. Contribution of environmental and spatial factors to the structure of stream fish assemblages at different spatial scales. Eco. Fresh. Fish. 23 (2), 208–223.
Pagliara, S., Kurdistani, S.M., 2017. Flume experiments on scour downstream of wood stream restoration structures. Geomorphology 279, 141–149.
Pease, A.A., GONZÁLEZ-DÍAZ, A.A., RODILES-HERNÁNDEZ, R.O.C.Í.O., Winemiller, K. O., 2012. Functional diversity and trait–environment relationships of stream fish assemblages in a large tropical catchment. Fresh. Bio. 57(5), 1060-1075.
Rosgen, D.L., 2006. The Cross-Vane, W-weir, and J-hook Structures: Description, Design and Application for Stream Stabilization and River Restoration. Wildland Hydrology, Colorado.
Rozovskiĭ, I.L., 1957. Flow of water in bends of open channels. Academy of Sciences of the Ukrainian SSR.
Shokrian Hajibehzad, M., Shafai Bejestan, M., Ferro, V., 2020. Investigating the performance of enhanced permeable groins in series. Water. 12 (12), 3531.
Teraguchi, H., Nakagawa, H., Kawaike, K., Yasuyuki, B.A.B.A., Zhang, H., 2011. Effects of hydraulic structures on river morphological processes. Int. J. Sediment. Res. 26 (3), 283–303.
Yeo, H.K., Kang, J.G., Kim, S.J., 2005. An experimental study on tip velocity and downstream recirculation zone of single groynes of permeability change. KSCE J. Civ. Eng. 9 (1), 29–38.
Zeng, J., Constantinescu, G., Weber, L., 2008. A 3D non-hydrostatic model to predict flow and sediment transport in loose-bed channel bends. J. Hydraul. Eng. 46 (5), 356–372.